

DOI: 10.1002/cbic.201200704

# Carnosine Inhibits A $\beta$ <sub>42</sub> Aggregation by Perturbing the H-Bond Network in and around the Central Hydrophobic Cluster

Francesco Attanasio,<sup>[a]</sup> Marino Convertino,<sup>[b]</sup> Andrea Magno,<sup>[b]</sup> Amedeo Caflich,<sup>[b]</sup> Alessandra Corazza,<sup>[c]</sup> Haritha Haridas,<sup>[c]</sup> Gennaro Esposito,<sup>[c]</sup> Sebastiano Cataldo,<sup>[d]</sup> Bruno Pignataro,<sup>[d]</sup> Danilo Milardi,<sup>\*[a]</sup> and Enrico Rizzarelli<sup>[a, e]</sup>

Aggregation of the amyloid- $\beta$  peptide (A $\beta$ ) into fibrillar structures is a hallmark of Alzheimer's disease. Thus, preventing self-assembly of the A $\beta$  peptide is an attractive therapeutic strategy. Here, we used experimental techniques and atomistic simulations to investigate the influence of carnosine, a dipeptide naturally occurring in the brain, on A $\beta$  aggregation. Scanning force microscopy, circular dichroism and thioflavin T fluorescence experiments showed that carnosine does not modify the conformational features of A $\beta$ <sub>42</sub> but nonetheless inhibits amyloid growth. Molecular dynamics (MD) simulations indicated that carnosine interacts transiently with monomeric A $\beta$ <sub>42</sub> by salt bridges with charged side chains, and van der Waals contacts with residues in and around the central hydrophobic cluster (<sup>17</sup>LVFFA<sup>21</sup>). NMR experiments on the nonaggregative fragment A $\beta$ <sub>12–28</sub> did not evidence specific intermolecular in-

teractions between the peptide and carnosine, in agreement with MD simulations. However, a close inspection of the spectra revealed that carnosine interferes with the local propensity of the peptide to form backbone hydrogen bonds close to the central hydrophobic cluster (residues E22, S26 and N27). Finally, MD simulations of aggregation-prone A $\beta$  heptapeptide segments show that carnosine reduces the propensity to form intermolecular backbone hydrogen bonds in the region 18–24. Taken together, the experimental and simulation results (cumulative MD sampling of 0.2 ms) suggest that, despite the inability of carnosine to form stable contacts with A $\beta$ , it might block the pathway toward toxic aggregates by perturbing the hydrogen bond network near residues with key roles in fibrillogenesis.

## Introduction

Alzheimer's disease (AD), the most common form of senile dementia, is a neurodegenerative disease characterized by the presence of neurofibrillary tangles and amyloid plaques in the brain.<sup>[1]</sup> The main constituents of the plaques are two peptides (40 and 42 amino acids long) called amyloid  $\beta$  peptides (A $\beta$ <sub>40</sub> and A $\beta$ <sub>42</sub>).<sup>[2]</sup> At first, attention was entirely focused on amyloid

fibrils as the cause of AD, but more recent studies have suggested that the small-sized, soluble A $\beta$  oligomers formed during the early steps of peptide aggregation are the main cytotoxic agents,<sup>[3]</sup> whereas A $\beta$  monomers show a neuroprotective role.<sup>[4]</sup> Although a causal relationship between the morphology of A $\beta$  aggregates and the severity of the disease remains open to discussion, considerable evidence indicates that a key event in AD pathogenesis is the conversion of A $\beta$  from its neuroprotective, soluble, monomeric state<sup>[4]</sup> into various toxic aggregated assemblies in the brain. Therefore, the design of effective molecules to prevent the self-assembly of A $\beta$  into toxic oligomers is widely recognized as the primary goal of a number of therapeutic strategies under development or in clinical trials. Despite the identification of oligomers as the critical pathogenic form of A $\beta$  aggregates, uncertainty concerning the structural features triggering toxic oligomerization persists due, in part, to the transient lifetimes of early intermediates and the dynamic transition into the thermodynamically favored fibrils. Recently, Ahmed et al. reported an A $\beta$ <sub>42</sub> fibril model with a turn spanning residues 24–27 in both oligomers and fibrils,<sup>[5]</sup> and a salt bridge connecting the side chains of residues D23 and K28 has been suggested as a hallmark of A $\beta$  aggregation.<sup>[6]</sup> Other reports have suggested that A $\beta$ <sub>42</sub>-medi-

[a] Dr. F. Attanasio,<sup>+</sup> Dr. D. Milardi, Prof. E. Rizzarelli  
Istituto di Biostrutture e Bioimmagini-UOS CT  
Consiglio Nazionale delle Ricerche  
V.le A. Doria 6, 95125 Catania (Italy)  
E-mail: dmilardi@unicat.it


[b] Dr. M. Convertino,<sup>+</sup> Dr. A. Magno, Prof. A. Caflich  
Biochemisches Institut, Universität Zürich  
Winterthurerstrasse 190, 8057 Zürich (Switzerland)

[c] Dr. A. Corazza,<sup>+</sup> Dr. H. Haridas, Prof. G. Esposito  
Dipartimento di Scienze Mediche e Biologiche, Università di Udine  
Piazzale Kolbe 4, 33100 Udine (Italy)

[d] Dr. S. Cataldo, Prof. B. Pignataro  
Dipartimento di Fisica e Chimica, Università di Palermo  
Viale delle Scienze, Parco d'Orleans II, Ed. 17, 90128 Palermo (Italy)

[e] Prof. E. Rizzarelli  
Dipartimento di Scienze Chimiche, Università degli Studi di Catania  
Viale A. Doria 6, 95125 Catania (Italy)

[<sup>+</sup>] These authors contributed equally to this work.

 Supporting information for this article is available on the WWW under <http://dx.doi.org/10.1002/cbic.201200704>.

ated toxicity is caused by a turn at positions E22 and D23 that favors the formation of toxic oligomers.<sup>[7]</sup>

Thus far, a number of diverse compounds have been used to prevent or reduce the aggregation of A $\beta$ , such as curcumin,<sup>[8]</sup> Congo Red derivatives,<sup>[9]</sup> antibodies,<sup>[10]</sup> osmolytes,<sup>[11]</sup> and peptidic  $\beta$ -sheet breakers,<sup>[12–14]</sup> but with limited success and often with dramatic side effects. Targeting amyloid toxicity by stimulating the endogenous protective responses of the cell might represent an attractive alternative, because this would make use of mechanisms that have evolved to specifically deal with amyloid toxic assemblies.

Carnosine ( $\beta$ -alanyl-L-histidine) is a naturally occurring dipeptide that is present in the muscle and brain tissues of humans and other vertebrates at relatively high concentrations (1–20 mM).<sup>[15,16]</sup> Although its physiological role is not fully established, this compound has been postulated to act as a proton buffer, metal chelator, antioxidant, and as an antiglycating and antiaggregating agent.<sup>[17–22]</sup> In vitro and in vivo

studies have revealed that carnosine can exert neuroprotective effects through various mechanisms. For example, it has been shown to protect neuronal cultures against glutamate-induced toxicity.<sup>[23,24]</sup> Carnosine has also been reported to protect PC12 cells from oxygen–glucose deprivation, thanks to its anti-oxidative properties.<sup>[25,26]</sup> Interestingly, carnosine has been shown to prevent A $\beta$ -amyloid aggregation in rat brain endothelial cells<sup>[27]</sup> and to rescue cells from A $\beta$ -induced neurotoxicity.<sup>[28–32]</sup> Furthermore, lower carnosine plasma levels have been found in AD patients than in age-matched controls.<sup>[33]</sup> Despite all these promising findings, however, no molecular interpretation is available as to how carnosine inhibits A $\beta$  amyloid toxicity. Indeed, investigating the molecular mechanism of the inhibition effects of carnosine on A $\beta$  aggregation would seem a highly promising challenge, as it might suggest novel lead compounds in anti-AD approaches.

In the present work, scanning force microscopy (SFM), circular dichroism (CD), and thioflavin T (ThT) fluorescence have provided consistent evidence that carnosine is able to inhibit A $\beta$ 42 aggregation and amyloid growth in the test tube without affecting its conformational preferences. However, these experimental approaches cannot provide a molecular description of how carnosine inhibits A $\beta$ 42 aggregation. Thus, implicit solvent molecular dynamics (MD) simulations were carried out to shed light on the specificity and persistence of the interactions between carnosine and monomeric A $\beta$ 42. Furthermore, 2D TOCSY and 2D NOESY NMR spectra of the water-soluble fragment A $\beta$ 12–28 were also recorded (in the absence and presence of carnosine) in experimental conditions designed to minimize A $\beta$ –A $\beta$  interactions. Based on our MD and NMR results, as well as previous biophysical experiments<sup>[34–37]</sup> and atomistic simulations,<sup>[38,39]</sup> we focused our investigation on the A $\beta$  region with the highest  $\beta$ -aggregation propensity, to obtain details about the A $\beta$  aggregation–inhibition mechanism. To this aim, additional MD simulations were performed

on eight replicates of each of the following capped heptapeptide segments: A $\beta$ 14–20, A $\beta$ 16–22, and A $\beta$ 18–24, in the absence (blank test) and presence of one single carnosine molecule. The simulations show van der Waals contacts between carnosine and several residues in the N-terminal half of A $\beta$ , as well as transient electrostatic interactions with residues K16, E22, and K28, with concomitant perturbation of the propensity to form intermolecular hydrogen bonds in region 18–24. The experimental data and simulation results provide evidence that binding of carnosine, albeit mainly transient, reduces the self-assembly tendency of A $\beta$ .

## Results

### Carnosine inhibits A $\beta$ 42 amyloid growth

Firstly, we studied whether carnosine could inhibit aggregation of A $\beta$ 42 by using a ThT assay (see the Experimental Section). The measurements were performed in 10 mM phosphate buffer (pH 7.4). A $\beta$ 42 samples were prepared and incubated without carnosine or in the presence of a 5-, 10-, 20-, or 100-fold molar excess of carnosine for four days at 37 °C. The inhibitory effect of carnosine on A $\beta$ 42 fibrillogenesis is shown in the upper panel of Figure 1.

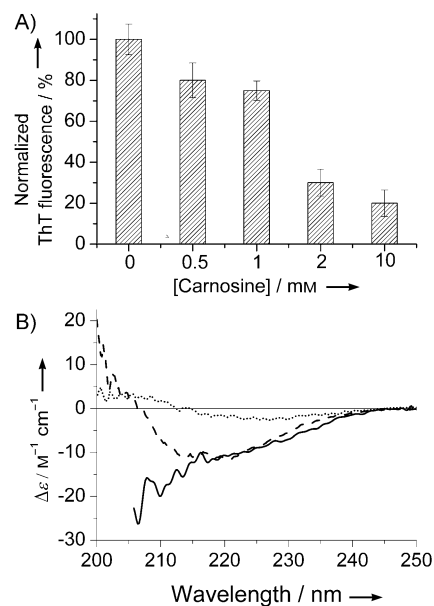


**Figure 1.** Top: normalized ThT fluorescence emission at 485 nm of samples containing 100  $\mu\text{M}$  A $\beta$ 42 incubated at 37 °C for four days in the presence of increasing concentrations of carnosine in 10 mM phosphate buffer (pH 7.4). Bottom: CD spectra of 15  $\mu\text{M}$  A $\beta$ 42 in 10 mM phosphate buffer (pH 7.4) at time  $t=0$  (—) and after incubation at 37 °C for four days in absence (····) or presence (----) of 0.1 mM carnosine. The dashed curve represents the difference spectrum obtained by subtracting the CD signal of carnosine from the CD curve of A $\beta$ 42 coincubated with 0.1 mM carnosine at 37 °C for four days.

The ThT results show that, at all the investigated concentrations, carnosine has a considerable effect on A $\beta$ 42 fibrillogenesis. In particular, at 20-fold molar excess carnosine exhibited a noticeable antiaggregating effect (70% reduction in fluores-

cence), and an 80% reduction was observed at a 100-fold molar excess. To analyze the effect of carnosine on the conformational behaviour of A $\beta$ 42, CD experiments were carried out in the presence of the dipeptide. CD spectra of carnosine alone were also acquired under the same experimental conditions and subtracted from the A $\beta$ 42/carnosine curves. The CD spectrum of A $\beta$ 42 obtained at time  $t=0$  showed that the peptide adopts a typical random-coil conformation (Figure 1B, solid line). After four days of incubation with carnosine, the spectrum exhibited a negative minimum at 220 nm, thus suggesting the presence of a  $\beta$ -sheet structure (Figure 1B, dashed line). The CD curve of pure A $\beta$ 42 (dotted line) exhibited similar spectral features but with a lower amplitude, ascribable to A $\beta$ 42 precipitation. These results confirm that the presence of carnosine does not significantly modify the conformational features of A $\beta$ 42 but, rather, interferes with its self-assembling process, thereby leading to a decrease in the total amount of fibrils formed at the end of the process. These findings were also demonstrated by SFM.

Figure 2A shows the two types of structure that characterize the morphology of A $\beta$ 42 on mica: fibrils and globular aggregates. Magnifications of these structures are shown in Figure 2B and C. In particular, Figure 2B shows a group of woven fibrils about 4 nm tall and 30–40 nm wide (the latter value was corrected for the well-known tip-broadening effect; see Experimental Section). Size distribution histograms of fibril lengths and aggregate heights (Figure 2D and E) were estimated over a large number of measurements in different regions of the sample. We observed that most of the fibrils were about 100–150 nm in length, although a small percentage reached some

microns (not shown). Globular aggregates were mostly less than 1 nm in diameter (range 0.5–6.0 nm). Given that the smallest aggregate was about 0.5 nm tall (and assuming this was for one monomer, as observed by SFM), this size distribution likely includes oligomers, or packed aggregates of monomers, composed of 1 to 10 units.

Figure 3 shows the SFM analysis of the A $\beta$ 42 sample treated with carnosine. A large number of globular structures randomly dispersed on the surface are evident. Importantly, fibril aggregation was limited to a very few systems. The aggregates are much more apparent in the 3D magnification (Figure 3B), and the related histogram (Figure 3C) shows a monodispersed height distribution ( $\sim 0.4$  nm), which, as above, is consistent with the presence of monomers or small oligomers.

### Interactions of carnosine with A $\beta$

Implicit solvent simulations were carried out on ten different systems (Table 1). At 300 K, carnosine was in contact with A $\beta$ 42 for only 20% of the simulation time (and only 10% with A $\beta$ 12–28)<sup>[40]</sup> at the concentration (5 mM) used in the simulations. Although the data at temperatures below 320 K were marred in part by incomplete convergence of sampling, it seems from analysis of the secondary structure that carnosine does not influence the overall secondary structure content of monomeric A $\beta$ 42 (Figure 4) or the secondary structure profile along the sequence (Figure S1 in the Supporting Information).

The profile of the interaction energies along the A $\beta$ 42 sequence indicates that van der Waals contacts are transient and significantly more pronounced in segment 3–22 than in the C-terminal region (Figure 5, top). Moreover, the electrostatic interactions (Figure 5, bottom) are rather promiscuous, with most of the positively and negatively charged side chains (including the terminal groups) of A $\beta$ 42 in transient contact with the carboxyl and amino group, respectively, of carnosine. Of note, the electrostatic interaction of carnosine with E22 is more pronounced than with the other negatively charged side chains (D1, E3, D7, and D23). This shows that, albeit disordered, the binding of carnosine to A $\beta$ 42 is influenced by sequence-specific effects.

### NMR characterization of A $\beta$ 12–28/carnosine contacts in solution

Ideally, to assess the presence of contacts between A $\beta$  and carnosine by NMR the full length peptide A $\beta$ 42 should be used. However, because of its poor solubility, A $\beta$ 42 is not suitable for NMR analysis in aqueous solvent. Because of this, and the interaction profile observed in the MD simulations with A $\beta$ 42, we used the small, water-soluble fragment A $\beta$ 12–28. We also focused on this central region of A $\beta$ 42 because it encompasses residues known to be critical for A $\beta$  aggregation.<sup>[6,41]</sup> Figure 6 depicts the overlay of the amide connectivity propagation from 2D

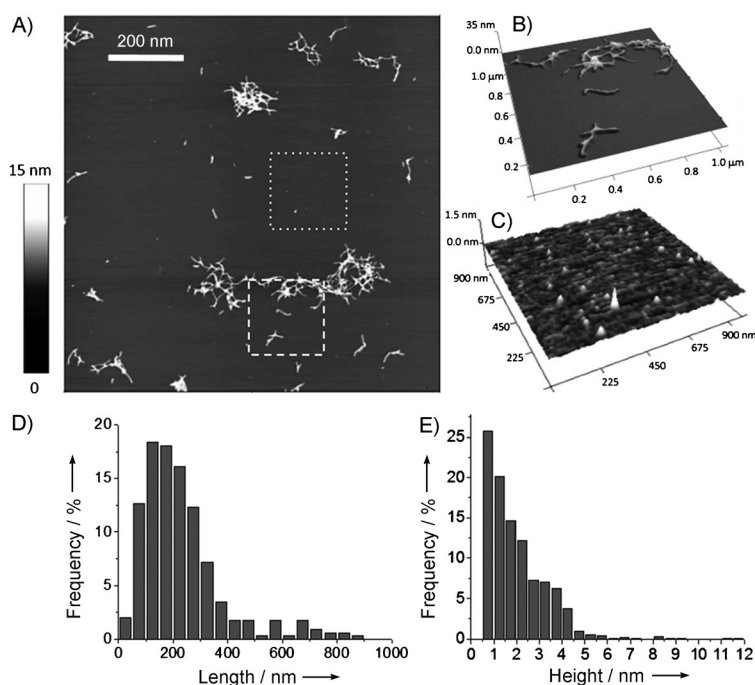


**Figure 2.** SFM analysis of the structures obtained by drop-casting a solution of A $\beta$ 42. A) 2D large-scale image; B) and C) 3D representations of the areas marked in (A) by dashed and dotted squares, respectively; D) length distributions of fibrils; E) height distributions of globular aggregates.

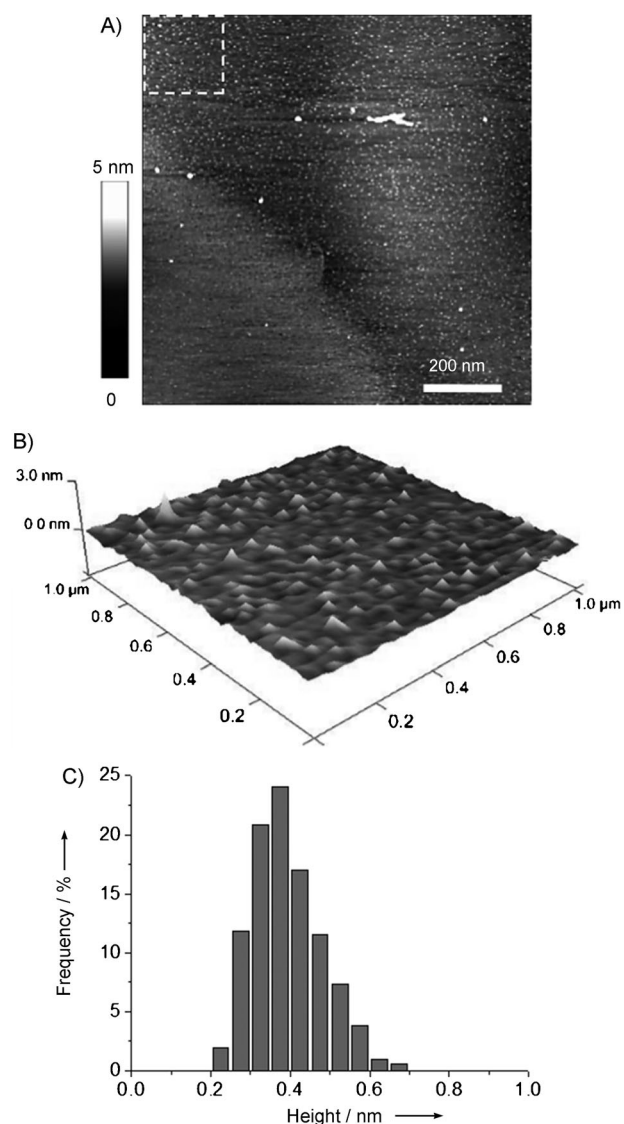


**Figure 3.** SFM analysis of the structures obtained by drop-casting solutions of A $\beta$ 42 and carnosine (0.1 and 10 mM, respectively). A) 2D large-scale image; B) 3D detail of the area marked in (A); C) height distribution of globular aggregates.

TOCSY spectra of A $\beta$ 12–28, alone and in the presence of carnosine (peptide/carnosine 1:2). For each stoichiometric equivalent addition of carnosine, the pH value increased progressively from 7.36 to 7.48, but no noteworthy shift was detected for the residues with carboxyl groups (E22, D23, and the C terminus). Chemical shift invariance with respect to carnosine additions was also observed for all the other resonances of A $\beta$ 12–28, including those of the aromatic hydrogens; this suggests lack of a stable interaction between the two molecules, or the existence of transient interactions not detectable within the timescale of NMR experiments. However, to better characterize the effect of carnosine on the peptide, the possible involvement of A $\beta$ 12–28 amide protons in H-bonding was ascertained by measuring the corresponding chemical shift thermal coefficients ( $\Delta\delta/\Delta T$ ) over the range 6.7–12 °C. The temperature-induced migration of the individual NH signals was reconstruct-

Table 1. Simulation parameters.						
Compound	A $\beta$ segment	Ratio	No. of runs	Length of each run [ $\mu$ s]	Protocol <sup>[a]</sup>	Total sampling at 300 K [ $\mu$ s]
carnosine	A $\beta$ 1–42	1:1	2	1.5	REMD <sup>[c]</sup>	3
–	A $\beta$ 1–42	0:1	2	1.5	REMD <sup>[c]</sup>	3
carnosine	A $\beta$ 12–28 <sup>[b]</sup>	1:1	3	5	CTMD	15
–	A $\beta$ 12–28 <sup>[b]</sup>	0:1	3	5	CTMD	15
carnosine	A $\beta$ 14–20	1:8	2	10	CTMD	20
–	A $\beta$ 14–20	0:8	2	10	CTMD	20
carnosine	A $\beta$ 16–22	1:8	2	10	CTMD	20
–	A $\beta$ 16–22	0:8	2	10	CTMD	20
carnosine	A $\beta$ 18–24	1:8	2	10	CTMD	20
–	A $\beta$ 18–24	0:8	2	10	CTMD	20

[a] REMD: replica exchange molecular dynamics; CTMD: constant temperature (300 K) molecular dynamics. [b] This simulation protocol is described in ref. [40]. [c] The temperatures of the individual replicas in REMD were 280, 290, 300, 310, 315, 320, 330, and 345 K.

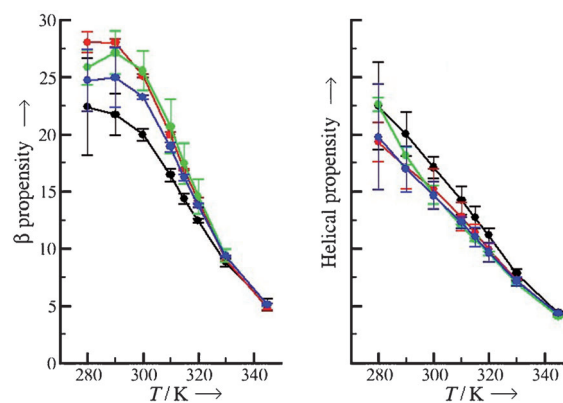


**Figure 4.** Secondary structure content [%] of monomeric A $\beta$ 42 (with (●, ●) and without (●, ●) carnosine, as a function of REMD simulation temperature. Data are plotted separately for two independent REMD runs for each of the two systems. Error bars represent the standard deviation calculated by block averaging at each temperature and run. The  $\beta$  propensity does not reach convergence below 320 K, as indicated by the significant deviation between the two REMD runs in the presence of carnosine. Overall, the temperature profiles indicate a negligible influence of carnosine on the tendency of A $\beta$ 42 to form regular elements of secondary structure.

ed from 2D TOCSY spectra. Table 2 lists the amide thermal coefficients with respect to carnosine presence: no difference is evident. The rather large  $\Delta\delta/\Delta T$  values (average  $(7.4 \pm 1.4)$  and  $(7.6 \pm 1.3)$  ppb per degree, without and with carnosine, respectively) are consistent with a lack of stable H-bonds. The lowest  $\Delta\delta/\Delta T$  values (at E22 and segment S26–N27) could be interpreted as reflecting a local trend towards H-bond formation, but somehow reduced by carnosine. The H $^{\alpha}$  chemical shifts, however (including those of S26 and N27) are very close to the values observed for statistically disordered peptides,<sup>[42]</sup> except for A21 and E22 where upfield shifts by 0.10 and 0.15 ppm were measured, independent of presence of carnosine. The H $^{\alpha}$  chemical shift deviations ( $\Delta\delta H^{\alpha}$ ) from the tabulated values for random structures are diagnostic for secondary structure re-



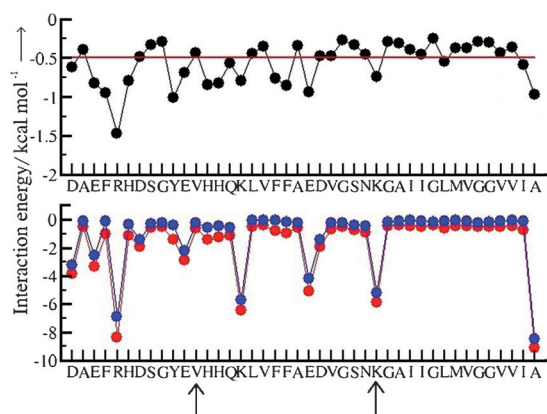


**Figure 5.** Interaction energy between carnosine and monomeric A $\beta$ 42 averaged over the REMD segments at 300 K (total sampling of 3  $\mu$ s). The two arrows highlight the segment A $\beta$ 12–28 used in the NMR spectroscopy experiments. Top: van der Waals interaction energy. The horizontal line at  $-0.5 \text{ kcal mol}^{-1}$  is a somewhat arbitrary threshold to help discriminate strongly from weakly interacting residues. Bottom: electrostatic (●) and total (●) interaction energies. The 300 K interaction energy profiles plotted separately for the two REMD runs show that these data are converged (Figure S8).

**Table 2.** Thermal coefficients ( $\Delta\delta/\Delta T$ ) in ppb per degree of A $\beta$ 12–28<sup>[a]</sup> amide hydrogen chemical shifts in the absence and presence of carnosine<sup>[a]</sup>, measured over the range 6.7–12 °C. The experimental error for all values is  $\pm 0.9$  ppb per degree.

Residue	$\Delta\delta/\Delta T$ [ppb/degree]	
	A $\beta$ 12–28	A $\beta$ 12–28 + carnosine
H13/H14	–6.9	–7.2
Q15/K16	–8.0	–8.9
L17	–9.1	–9.8
V18	–8.8	–8.8
F19	–9.4	–9.3
F20	–7.3	–7.4
A21	–6.6	–6.9
E22	–6.2	–6.5
D23	–6.9	–7.2
V24	–9.0	–8.8
G25	–7.0	–7.3
S26	–5.8	–6.1
N27	–4.8	–5.5
K28	–6.8	–6.8

[a] A $\beta$ 12–28 0.46 mM in 92:8 H<sub>2</sub>O/D<sub>2</sub>O, 16 mM phosphate and 4 mM NaOH, at pH 7.36. On addition of 0.95 mM carnosine, pH increased to 7.48. For the unresolved H13/H14/D23 and Q15/K16 amide crosspeaks (Figure 6), single  $\Delta\delta/\Delta T$  values were determined.

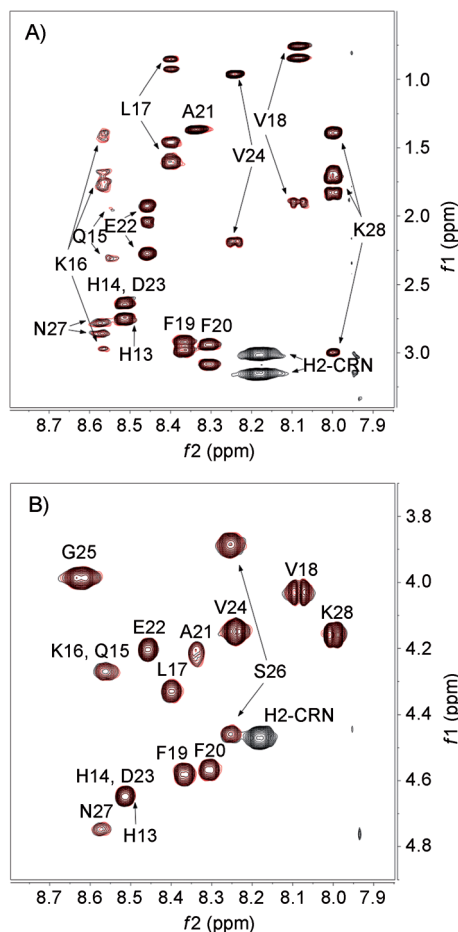


**Figure 6.** 2D <sup>1</sup>H TOCSY regions of 0.46 mM A $\beta$ 12–28 in H<sub>2</sub>O/D<sub>2</sub>O (92:8) with 4 mM NaOH and 16 mM phosphate (pH 7.36) at 6.7 °C, in the absence (red) and in the presence (black) of 0.95 mM carnosine (CRN). A) The amide connectivities to the  $\alpha$ CHs (and  $\beta$ CH<sub>2</sub> for S26); B) the propagation to the other resonances of the spin systems. Under these conditions, excess carnosine raised the pH to 7.48, but no shift was detected for E22, D23, or K28 connectivities.

gions when not below 0.1 ppm and when occurring as consecutive groups.

However, based on the evidence from NOESY data (Figure 7), it is possible to attribute a structural meaning to the upfield deviations detected for A21 and E22: bending into a local  $\alpha$ -like conformation that introduces a loose turn geometry. To investigate the possibility of peptide–carnosine association phenomena, we performed DOSY measurements in aqueous phosphate.

The results of these experiments are reported in Table 3 in terms of the hydrodynamic radii ( $R_h$ ) of A $\beta$ 12–28 and carnosine, calculated according to a procedure reported elsewhere.<sup>[43]</sup> From these data, we can confirm that, with or without carnosine, A $\beta$ 12–28 is predominantly monomeric in aqueous phosphate at neutral pH and low temperature.

The apparent  $R_h$  value of carnosine increases in the presence of A $\beta$ 12–28 because of the transient fast interaction. Although less pronounced, the A $\beta$ 12–28 diffusion coefficient (and hence the apparent  $R_h$  value) is also affected by the fast intermolecular interaction. Sample aging did not alter significantly the monomeric state of A $\beta$ 12–28, at least over three to four weeks, independently of the presence of carnosine. In fact, the  $R_h$  values are constant.

The monomeric state of A $\beta$ 12–28 is not affected by temperature. In fact, no aggregation due to hydrophobic interactions (in principle favored with increasing temperature) can be inferred from the  $R_h$  values at higher temperatures. Rather, a decrease in these values was observed at higher temperatures, which should be determined by fast conformational dynamics resulting in changes in the average hydrodynamic dimensions of A $\beta$ 12–28. The failure to observe all the amide resonances in the spectra acquired at  $T \geq 25$  °C (because of the fast solvent exchange expected above neutral pH) is consistent with a stat-

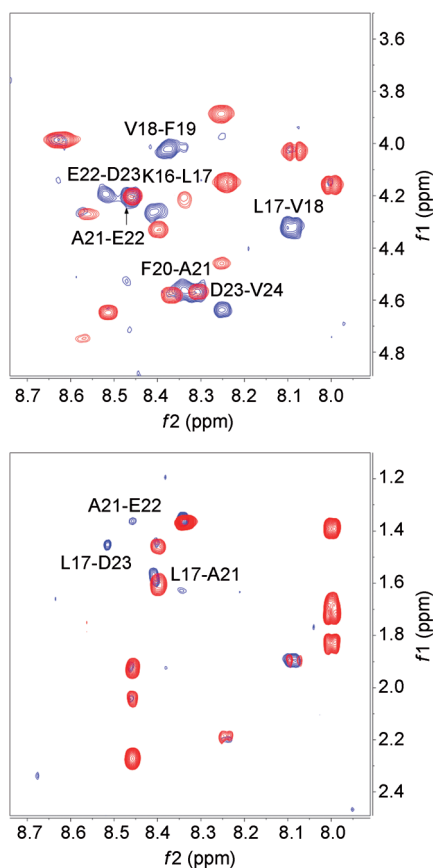


**Figure 7.** Overlay of 2D TOCSY (red) and 2D NOESY (blue) regions of 0.46 mM A $\beta$ 12–28 in H<sub>2</sub>O/D<sub>2</sub>O (92:8) with 4 mM NaOH and 16 mM phosphate (pH 7.36) at 6.7 °C. A) The intense H $\alpha$ –HN connectivities; B) H $\beta$ –HN connectivities. It is worth noting that all these connectivities occur within segment L17–V24.

istical conformational averaging. In accordance with the NMR analysis, MD simulations of the A $\beta$ 12–28 peptide evidenced that carnosine interacts mainly with the E22, K16, and K28 side chains of A $\beta$ 12–28, and that all these interactions are short-lived<sup>[40]</sup> (Figures S2 and S3). The decomposition of intermolecular energy into contributions of individual pairs of functional groups illustrates that the main interactions involve formal charges of opposite sign, that is, the N-terminal amino group of carnosine with E22 and D23 side chains, and the C-terminal carboxy group of carnosine with K16 and K28 side chains.

### Molecular dynamics simulations of octameric A $\beta$ heptapeptides with carnosine

The following analysis is based on MD simulations at 300 K of six systems: octameric A $\beta$ 14–20, octameric A $\beta$ 16–22, and octameric A $\beta$ 18–24, each of these three systems with and without one molecule of carnosine (Table 1).

The total sampling for each of the octameric heptapeptide system was 20  $\mu$ s. A comparison of the distribution of the number of interpeptide backbone hydrogen bonds in the MD simulations with and without carnosine shows that the dipeptide reduces the aggregation tendency of the octameric A $\beta$ 18–

**Table 3.** Hydrodynamic radii ( $R_h$ ) of A $\beta$ 12–28<sup>[a]</sup> and carnosine measured as a function of temperature and sample age.

T [°C]	$R_h$ A $\beta$ 12–28 [nm]	$R_h$ carnosine [nm]	Sample age [d]
6.7	1.04 $\pm$ 0.09	–	1
6.7	1.04 $\pm$ 0.06	0.38 $\pm$ 0.02	1
6.7	–	0.34 $\pm$ 0.01	1
6.7	0.97 $\pm$ 0.05	–	7
6.7	0.98 $\pm$ 0.06	0.40 $\pm$ 0.03	7
6.7	0.99 $\pm$ 0.03	–	20
6.7	1.01 $\pm$ 0.03	0.40 $\pm$ 0.03	20
12	0.96 $\pm$ 0.01	–	21
12	0.99 $\pm$ 0.02	0.37 $\pm$ 0.01	21
25	0.92	–	28
25	0.92	0.37	28
30	0.93	–	28
30	0.93	0.37	28

[a] A $\beta$ 12–28 0.46 mM in 92:8 H<sub>2</sub>O/D<sub>2</sub>O, 16 mM phosphate, and 4 mM NaOH, at pH 7.36. When 0.95 mM carnosine was present, the pH increased to 7.48. The  $R_h$  values were determined from the average diffusion coefficients determined by single exponential fitting of different A $\beta$ 12–28 methyl signals and the  $\beta$ -alanine methylene signals of carnosine.  $R_h$  uncertainties are the standard deviations calculated from the dispersion of the diffusion coefficients. The values at 25 and 30 °C were obtained from the diffusion coefficients estimated directly from the corresponding DOSY maps. In this case uncertainty should be 5–10%, as the  $R_h$  of TSP (the NMR chemical shift internal reference) was 0.29 nm at both temperatures, thus ensuring the reliability of the determinations.

24 system significantly, but only marginally for octameric A $\beta$ 14–20 and A $\beta$ 16–22 (Figure 8, top, see also the time series in Figures S4 and S5). The number of intra-peptide backbone hydrogen bonds increased significantly only for the A $\beta$ 18–24 heptapeptide (Figure 8F) which is consistent with the decrease in interpeptide hydrogen bonds. The change in the distribution of the interpeptide interaction energy (Figure 8, bottom) confirms that carnosine has a minor effect on the mainly  $\beta$ -sheet aggregates of the octameric A $\beta$ 14–20 and A $\beta$ 16–22 systems while it has a stronger influence, that is, larger shift to less favorable values, for octameric A $\beta$ 18–24. Note that the distributions shown in Figure 8 are not affected by statistical error as shown by block averaging in Figure S6. The short residence time of carnosine on A $\beta$ 42 and on the A $\beta$  heptapeptide systems indicate that the intermolecular interactions are weak and exhibit a transient nature (see Figures S3, S4 and S7).

## Discussion

Carnosine, a naturally occurring dipeptide, is becoming a clinically accepted nutritional supplement with uses across a considerable spectrum of chronic diseases, from senile cataract to dementia. It is found in excitable tissues such as the myocardium, skeletal muscles and brain, but it is normally destroyed by the enzyme carnosinase. Normally, carnosinase acts fast and reduces the serum levels of carnosine, thus diminishing its effectiveness in clinical treatments.<sup>[21]</sup> There have been attempts at stabilizing carnosine against carnosinase degradation, for example, by conjugating it with vitamin E derivatives<sup>[44]</sup> or small sugars,<sup>[45,46]</sup> but research in this area is still underway. It is

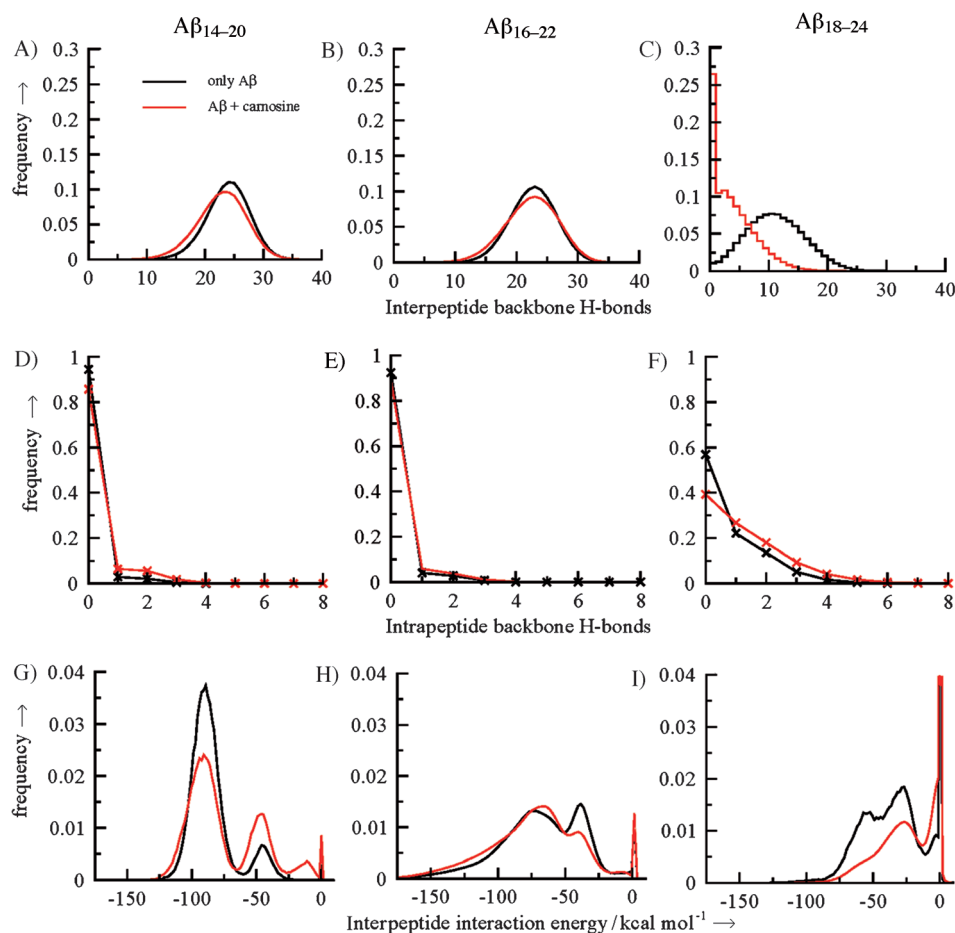


**Figure 8.** Influence of carnosine on the interpeptide hydrogen bonds (top graphs), intrapeptide hydrogen bonds (middle), and interpeptide interaction energy (bottom) in the octameric Aβ heptapeptide systems. Each distribution was calculated from the complete sampling (20 μs). The statistical error is much smaller than the difference between the distributions with and without carnosine (see Figure S6).

known that carnosine can protect cells exposed to high levels of Aβ<sub>42</sub> and it has been postulated that the mechanism for protection might lie in its anti-glycating, antioxidant and/or metal-chelating activities. Inspired by the consistent body of evidence supporting a neuroprotective activity of carnosine,<sup>[47]</sup> we show here that millimolar concentrations of this dipeptide are able to effectively hinder Aβ growth in tube tests. This property of carnosine could be particularly important as direct interference with Aβ aggregation is a major target in AD therapeutics,<sup>[48]</sup> especially as a nutraceutical antagonist of Aβ self-assembly<sup>[49]</sup> has recently reached the phase II clinical trial step. On the other hand, the recent failure of the small molecule tramiprosate in phase III clinical trials calls for novel inhibitors with alternative mechanisms of modulation of Aβ aggregation.<sup>[48]</sup> Carnosine/Aβ interactions are weak and characterized by short-lived contacts localized around the central hydrophobic cluster of Aβ. These interactions do not significantly affect the conformational preferences of Aβ<sub>42</sub>. Consistent with biophysical experiments and MD simulations, NMR spectra of the fragment Aβ<sub>12-28</sub> showed that the upfield shifts of the signals from A21 and E22, which are ascribable to local loose turn geometries, are not affected by carnosine. However, a closer in-

spection of NMR spectra collected at different temperatures could be interpreted as a local trend towards H-bond formation in E22 and in the segment S26–N27 being reduced by carnosine.

Consistent with NMR data, MD simulations of heptapeptide segments of Aβ show a significant decrease of the number of interpeptide H-bonds in the region 18–24. Notably, a toxic conformer of Aβ<sub>42</sub> with a turn at positions 22 and 23 (the toxic turn) has recently been identified by solid-state NMR, and it was demonstrated that a monoclonal antibody against the toxic turn mainly detected Aβ oligomers in the brains of AD patients.<sup>[7]</sup> Moreover, the salt bridge between the side chains of D23 and K28 is also known to play a critical role in Aβ toxicity, and agents that drive these residues towards non-salt-bridge-forming conformations are thought to have therapeutic applications in AD.<sup>[50]</sup> Our data support the hypothesis that, albeit transiently, carnosine interacts with the charged groups surrounding the central hydrophobic cluster of Aβ and interferes with the network of H-bonds near the turn

at positions 22 and 23, thereby hindering self-assembly. Our results, along with analogous studies, might explain in part the beneficial effect of carnosine (or derivatives thereof) in the treatment of AD.

## Experimental Section

**Chemicals:** Aβ<sub>42</sub> and Aβ<sub>12-28</sub> were purchased from Anaspec (Fremont, CA). Carnosine, trifluoroacetic acid (TFA) and 1,1,1,3,3,3-hexafluoropropan-2-ol (HFIP) were from Sigma–Aldrich. The purity of all peptides was >95%. All other chemicals were of the highest available grade and were used without further purification. Ultrapure, metal-free Milli-Q water (EMD Millipore, Billerica, MA) was used in all experiments.

**Aβ peptide preparation and analysis:** Monomeric Aβ<sub>42</sub> was prepared as reported elsewhere.<sup>[51,52]</sup> The peptide was initially dissolved in TFA (1 mg mL<sup>-1</sup>) and sonicated in a water bath for 10 min. Then, TFA was evaporated under a gentle stream of argon and HFIP (1 mL) was added. After incubation (37 °C, 1 h), the peptide solution was dried under a stream of argon, and then solubilized again by adding HFIP (2 mL). Finally, HFIP was removed in an argon stream, followed by drying in a lyophilizer for 1 h. The dried peptide was first dissolved in freshly prepared NaOH (2 mM), then

the appropriate volume of phosphate buffer (10 mM, pH 7.4) was added to a final peptide concentration of 100  $\mu\text{M}$ . A $\beta$ 42 samples without and with carnosine were incubated for four days at 37  $^{\circ}\text{C}$ .

**Circular dichroism:** The CD spectra of the A $\beta$ 42 sample (15  $\mu\text{M}$  in phosphate buffer (10 mM, pH 7.4)) at time  $t=0$  and after incubation at 37  $^{\circ}\text{C}$  for four days in the absence or presence of carnosine (0.1 mM) were recorded at 25  $^{\circ}\text{C}$  on a J-810 spectropolarimeter (Jasco), thermostated with a Jasco peltier accessory. Raw CD data acquired in a quartz cell (path length 10 mm) were processed by Spectra Manager 1.5 software (Jasco) and corrected by subtraction of the background solvent spectrum obtained under identical experimental conditions. The final CD curves represent averages of ten spectra.

**ThT fluorescence measurements:** Fluorescence emission spectra of ThT undergo a red shift upon incorporation into  $\beta$ -sheet amyloid structures. Aliquots of incubated A $\beta$ 42 peptide (100  $\mu\text{M}$ ) with different amounts of carnosine, were added to ThT in phosphate buffer (10 mM, pH 7.4); final concentrations: 30  $\mu\text{M}$  ThT, 10  $\mu\text{M}$  A $\beta$ 42. Fluorescence emission spectra were recorded in a quartz cell (light path of 1 cm) by an LS55 spectrofluorimeter ( $\lambda_{\text{ex}}=440$  nm; PerkinElmer). Excitation and emission bandwidths were set to 5 nm. ThT spectra were corrected by subtraction of the background solvent spectrum obtained under identical experimental conditions. Ten consecutive spectra were recorded and averaged; the experiments were performed in triplicate. Emission at 485 nm was plotted as function of carnosine concentration.

**Scanning force microscopy:** Samples were prepared by drop casting A $\beta$ 42 (100  $\mu\text{M}$ , 5  $\mu\text{L}$ ) or A $\beta$ 42/carnosine (100  $\mu\text{M}$ /10 mM, 5  $\mu\text{L}$ ) onto a freshly cleaved mica surface and incubating for 5 min. Surfaces were then rinsed with ultrapure Milli-Q water and dried with a stream of dry nitrogen. SFM imaging was performed with a Multi-mode/Nanoscope IIIA (Bruker, Santa Barbara, CA) with commercially available etched-silicon Vista probes (nanoScience Instruments, Phoenix, AZ). For each image, 512 $\times$ 512 points were collected (scan rate 1 Hz). To get dimensional data for proteins, we used mainly height data. This is because it is well-known that the SFM lateral investigation of nanostructures is affected by the "tip-broadening effect".<sup>[53]</sup> Accordingly, tip/surface convolution leads to broadening of more than 10 nm, as typically observed by conventional SFM probes for structures (e.g., proteins) that are few nanometers in size.<sup>[54,55]</sup> The following algorithm can be used to compensate for tip broadening:

$$W_{\text{obs}} = 4\sqrt{\frac{W}{2}} \times R_{\text{tip}}$$

where  $W_{\text{obs}}$  and  $W$  are the observed and real width respectively and  $R_{\text{tip}}$  is the tip radius.<sup>[56]</sup> Particle height and fiber length data were recorded by Nanoscope software and then gathered into a single data set and statistically analyzed with Origin 8 software. Distribution histograms were obtained from hundreds of elements.

**Molecular dynamics:** Implicit solvent simulations were performed with ten different systems (Table 1). Six simulation systems had eight copies each of the capped heptapeptides A $\beta$ 14–20, A $\beta$ 16–22, or A $\beta$ 18–24, both in absence or presence of a single carnosine molecule (8:1 ratio). The remaining four systems consisted of monomeric A $\beta$ 42 or monomeric A $\beta$ 12–28 without or with carnosine (1:1 ratio). All A $\beta$  peptide segments were capped by acetyl and *N*-methylamide groups at the N- and C-terminal residues, respectively, to avoid spurious charges not present in full length A $\beta$ 42. All simulations were performed with the CHARMM program;<sup>[57,58]</sup> pep-

tides and carnosine were modeled by using the united atoms CHARMM PARAM19 force field with its default truncation scheme for nonbonding interaction (cutoff 7.5  $\text{\AA}$ ). Protonation states of titratable residues were considered at pH 7.0; in particular, the imidazole of carnosine was neutral (protonated at N $\delta$ ) while its amino and carboxy groups were treated as positively and negatively charged, respectively. The electrostatic contribution to solvation was accounted for by using FACTS, an efficient generalized Born implicit solvent model, which is based on the fully analytical evaluation of the volume and spatial symmetry of the solvent that is displaced from around a solute atom by its neighboring atoms.<sup>[59]</sup> The nonpolar contributions to solvation energy was approximated by a term proportional to the surface of the solute, by using a surface-tension-like, multiplicative parameter (0.0075 kcal mol $^{-1}$   $\text{\AA}^{-2}$ ). The simulations were prepared by initially placing eight monodispersed replicates of the same heptapeptide (for the octameric systems) or one A $\beta$ 42 or A $\beta$ 12–28 peptide (for the monomeric systems), with or without a single carnosine molecule in the simulation box. Note that the initial relative positions and orientations are irrelevant because of the length of the individual trajectories (each of several microseconds), which yielded multiple association/dissociation events. Simulations were carried out with a periodic boundary condition and at a fixed peptide concentration (4.88 mM; the simulation boxes were set to 132  $\text{\AA}$  for A $\beta$ 14–20, A $\beta$ 16–22, and A $\beta$ 18–24, and to 69  $\text{\AA}$  for A $\beta$ 42 and A $\beta$ 12–28) with a Langevin integrator at low friction (coefficient 0.15 ps $^{-1}$ ). The octameric heptapeptide systems were simulated at 300 K, which yielded reversible aggregation. The same temperature was used for the A $\beta$ 12–28 segment. The simulations of full length A $\beta$ 42 with and without carnosine were conducted with the Replica Exchange Molecular Dynamics (REMD) technique at the temperatures listed in Table 1. Every 20 ps, states  $i$  and  $j$  from neighboring temperatures were swapped according to a Metropolis-like algorithm; this yielded an average acceptance ratio of 40% for temperature swaps. For each octameric system, ten 2  $\mu\text{s}$  runs were carried out, starting from randomly placed heptapeptides without any intermolecular interaction. Analogously, simulations in the presence of carnosine were started without any contact between carnosine and A $\beta$  (full length or segment). The cumulative MD sampling at 300 K was 156  $\mu\text{s}$  (198  $\mu\text{s}$  when considering REMD sampling at different temperatures; Table 1).

**Analysis of trajectories:** The interaction energy of carnosine with A $\beta$ 42 was calculated with CHARMM, with the same threshold as for the simulations (7.5  $\text{\AA}$ ). The program Wordom<sup>[60,61]</sup> was employed to calculate secondary-structure propensities according to the DSSP algorithm.<sup>[62]</sup> Carnosine influence on the ordered aggregation of octameric A $\beta$ 14–20, A $\beta$ 16–22, and A $\beta$ 18–24 was analyzed by the average number of inter- and intrapeptide H-bonds and their distributions along the simulations for each studied system. The following hydrogen bond criteria were employed: distance threshold 2.5  $\text{\AA}$  for the H–O distance, and cut off  $>130^{\circ}$  for the NH–O angle. The carnosine effect on A $\beta$  heptapeptide aggregation was estimated by calculating the interpeptide interaction energy, which is the CHARMM nonbonded energy (van der Waals plus electrostatic) of a single A $\beta$  peptide with the remaining seven peptides, without considering the carnosine molecule.

**NMR measurements:** All NMR experiments were carried out at 11.7 T in an Avance 500 spectrometer (Bruker) equipped with triple-axis magnetic field gradients, by observing the hydrogen spectrum at 500.13 MHz. To avoid A $\beta$ 12–28 aggregation and precipitation, the peptide was first dissolved under basic conditions (2.3 mM in NaOH (20 mM), pH  $>10$ ).<sup>[63]</sup> Fivefold dilution in phos-



phate buffer led to final concentrations of peptide, phosphate, and NaOH of 0.46, 16, and 4 mM, respectively, in H<sub>2</sub>O/D<sub>2</sub>O (92:8, pH 7.36). Carnosine additions were performed with aliquots (5–10  $\mu$ L) from a stock solution in phosphate buffer (50 mM, pH 7.42)) to reach stoichiometric ratios 1:1 and 2:1 (carnosine:A $\beta$ 12–28), with a final pH of 7.48. To inhibit hydrophobic interaction, all operations were performed in an ice bath, and solutions were stored at 4 °C. For NMR measurements, the temperature was set initially to 6.7 °C and subsequently increased stepwise: 6.7–12 °C, then 25–30 °C. Chemical shifts were referenced to internal 3-trimethyl-silyl 2,2,3,3-tetradeutero sodium propionate (TSP). In addition to 1D spectra, 2D TOCSY<sup>[64]</sup> and NOESY<sup>[65]</sup> experiments were performed, typically with 2048  $\times$  512 ( $t_2 \times t_1$ ) data-point matrices for spectral widths of 6 kHz in each dimensions with 64 scans per  $t_1$  point, 64 dummy scans, and relaxation delay of 1 s. The TOCSY MLEV17<sup>[66]</sup> isotropic mixing intervals were 80 ms at  $\gamma B_2/2\pi = 8.3$  kHz; for NOESY, mixing times of 250 ms were employed. Quadrature in the indirect dimension was obtained by time-proportional phase incrementation,<sup>[67]</sup> and solvent suppression was implemented by appending a WATERGATE spin-echo module to the sequences, performed in the excitation-sculpting mode.<sup>[68,69]</sup> This solvent suppression scheme was also used in diffusion ordered spectroscopy (DOSY)<sup>[70]</sup> experiments for the measurement of the diffusion coefficients. A sequence including bipolar gradients and longitudinal eddy current suppression was employed in a double-stimulated echo module delay for cancellation of convection artifacts,<sup>[71]</sup> to collect 80 points with linear increments from 2 to 95% of the z-axis magnetic field gradient (65 G cm<sup>-1</sup>), with delays  $\Delta = 90$  ms,  $\sigma = 2 \times 2$  ms, and 128 scans/increment. All data were processed with TOPSPIN software (Bruker).

## Acknowledgements

This work was supported by MIUR (grants: PRIN 2010M2JARJ\_001; PRIN 20083ERXWS\_005; FIRB-MERIT no. RBNE08HWLZ\_010). M.C. and A. Caflich are grateful to Riccardo Pellarin, Andreas Vitalis and the late François Marchand for interesting discussions. The simulations were carried out on the Schrodinger cluster of the University of Zürich. The work in Zürich was supported financially by the Swiss National Science Foundation and the Swiss National Competence Center (NCCR) on Neural Plasticity and Repair.

**Keywords:** Alzheimer's disease • carnosine • molecular dynamics • neuroprotective agent • nutraceutical compounds • protein–protein interactions

- [1] J. Hardy, *Neurobiol. Aging* **2002**, *23*, 1073–1074.
- [2] J. Kang, H.-G. Lemaire, A. Unterbeck, J. M. Salbaum, C. L. Masters, K.-H. Grzeschik, G. Multhaup, K. Beyreuther, B. Müller-Hill, *Nature* **1987**, *325*, 733–736.
- [3] C. Haass, D. J. Selkoe, *Nat. Rev. Mol. Cell Biol.* **2007**, *8*, 101–112.
- [4] M. L. Giuffrida, F. Caraci, B. Pignataro, S. Cataldo, P. De Bona, V. Bruno, G. Molinaro, G. Pappalardo, A. Messina, A. Palmigiano, D. Garozzo, F. Nicoletti, E. Rizzarelli, A. Copani, *J. Neurosci.* **2009**, *29*, 10582–10587.
- [5] M. Ahmed, J. Davis, D. Aucoin, T. Sato, S. Ahuja, S. Aimoto, J. I. Elliott, W. E. Van Nostrand, S. O. Smith, *Nat. Struct. Mol. Biol.* **2010**, *17*, 561–567.
- [6] K. L. Sciarretta, D. J. Gordon, A. T. Petkova, R. Tycko, S. C. Meredith, *Biochemistry* **2005**, *44*, 6003–6014.
- [7] N. Izuo, T. Kume, M. Sato, K. Murakami, K. Irie, Y. Izumi, A. Akaie, *ACS Chem. Neurosci.* **2012**, *3*, 674–681.
- [8] A. N. Begum, M. R. Jones, G. P. Lim, T. Morihara, P. Kim, D. D. Heath, C. L. Rock, M. A. Pruitt, F. Yang, B. Hudspeth, S. Hu, K. F. Faull, B. Teter, G. M. Cole, S. A. Frautschy, *J. Pharmacol. Exp. Ther.* **2008**, *326*, 196–208.
- [9] P. Frid, S. V. Anisimov, N. Popovic, *Brain Res. Rev.* **2007**, *53*, 135–160.
- [10] B. Solomon, *Curr. Opin. Invest. Drugs* **2007**, *8*, 519–524.
- [11] D.-S. Yang, C. M. Yip, T. H. J. Huang, A. Chakrabarty, P. E. Fraser, *J. Biol. Chem.* **1999**, *274*, 32970–32974.
- [12] P. Soto, M. A. Griffin, J.-E. Shea, *Biophys. J.* **2007**, *93*, 3015–3025.
- [13] C. Soto, E. M. Sigurdsson, L. Morelli, R. A. Kumar, E. M. Castaño, B. Frangione, *Nat. Med.* **1998**, *4*, 822–826.
- [14] P. De Bona, M. L. Giuffrida, F. Caraci, A. Copani, B. Pignataro, F. Attanasio, S. Cataldo, G. Pappalardo, E. Rizzarelli, *J. Pept. Sci.* **2009**, *15*, 220–228.
- [15] R. Kohen, Y. Yamamoto, K. C. Cundy, B. N. Ames, *Proc. Natl. Acad. Sci. USA* **1988**, *85*, 3175–3179.
- [16] J. J. O'Dowd, D. J. Robins, D. J. Miller, *Biochim. Biophys. Acta Gen. Subj.* **1988**, *967*, 241–249.
- [17] H. Abe, *Biochemistry (Moscow)* **2000**, *65*, 757–765.
- [18] A. R. Hipkiss, J. E. Preston, D. T. M. Himsworth, V. C. Worthington, M. Keown, J. Michaelis, J. Lawrence, A. Mateen, L. Allende, P. A. M. Eagles, N. J. Abbott, *Ann. N. Y. Acad. Sci.* **1998**, *854*, 37–53.
- [19] F. Attanasio, S. Cataldo, S. Fischella, S. Nicoletti, V. G. Nicoletti, B. Pignataro, A. Savarino, E. Rizzarelli, *Biochemistry* **2009**, *48*, 6522–6531.
- [20] V. Calabrese, E. Guagliano, M. Sapienza, A. Ravagna, V. Cardile, G. Scapagnini, A. M. Santoro, A. Mangiameli, D. A. Butterfield, A. M. Giuffrida Stella, E. Rizzarelli, *Neurochem. Res.* **2005**, *30*, 797–807.
- [21] F. Bellia, G. Vecchio, E. Rizzarelli, *Amino Acids* **2012**, *43*, 153–163.
- [22] V. Calabrese, C. Cornelius, S. Cuzzocrea, I. Iavicoli, E. Rizzarelli, E. J. Calabrese, *Mol. Aspects Med.* **2011**, *32*, 279–304.
- [23] A. Boldyrev, E. Bulygina, T. Leinsoo, I. Petrushanko, S. Tsubone, H. Abe, *Comp. Biochem. Physiol. Part B* **2004**, *137*, 81–88.
- [24] A. Boldyrev, R. Song, D. Lawrence, D. O. Carpenter, *Neuroscience* **1999**, *94*, 571–577.
- [25] R. Tabakman, H. Jiang, R. A. Levine, R. Kohen, P. Lazarovici, *Neurosci. Res.* **2004**, *75*, 499–507.
- [26] F. Bellia, G. Vecchio, S. Cuzzocrea, V. Calabrese, E. Rizzarelli, *Mol. Aspects Med.* **2011**, *32*, 258–266.
- [27] J. E. Preston, A. R. Hipkiss, D. T. M. Himsworth, I. A. Romero, J. N. Abbott, *Neurosci. Lett.* **1998**, *242*, 105–108.
- [28] Q. Fu, H. Dai, W. Hu, Y. Fan, Y. Shen, W. Zhang, Z. Chen, *Cell. Mol. Neurobiol.* **2008**, *28*, 307–316.
- [29] H. Atamna, R. Kumar, *J. Alzheimer's Dis.* **2010**, *20*, S439–S452.
- [30] X. Fernández-Busquets, J. Ponce, R. Bravo, M. Arimon, T. Martiáñez, A. Gella, J. Cladera, N. Durany, *Curr. Alzheimer Res.* **2010**, *7*, 428–438.
- [31] A. R. Hipkiss, *J. Alzheimer's Dis.* **2007**, *11*, 229–240.
- [32] A. Boldyrev, A. Koudinov, T. Berezov, D. O. Carpenter, *J. Alzheimer's Dis.* **2004**, *6*, 633–638.
- [33] A. N. Fonteh, R. J. Harrington, A. Tsai, P. Liao, M. G. Harrington, *Amino Acids* **2007**, *32*, 213–224.
- [34] L. O. Tjernberg, J. Näslund, F. Lindqvist, J. Johansson, A. Karlström, J. Thyberg, L. Terenius, C. Nordstedt, *J. Biol. Chem.* **1996**, *271*, 8545–8548.
- [35] A. D. Williams, E. Portelius, I. Kheterpal, J.-t. Guo, K. D. Cook, Y. Xu, R. Wetzel, *J. Mol. Biol.* **2004**, *335*, 833–842.
- [36] F. T. Senguen, N. R. Lee, X. Gu, D. M. Ryan, T. M. Doran, E. A. Anderson, B. L. Nilsson, *Mol. Biosyst.* **2011**, *7*, 486–496.
- [37] F. T. Senguen, T. M. Doran, E. A. Anderson, B. L. Nilsson, *Mol. Biosyst.* **2011**, *7*, 497–510.
- [38] M. Cecchini, R. Curcio, M. Pappalardo, R. Melki, A. Caflich, *J. Mol. Biol.* **2006**, *357*, 1306–1321.
- [39] A. Caflich, *Curr. Opin. Chem. Biol.* **2006**, *10*, 437–444.
- [40] M. Convertino, A. Vitalis, A. Caflich, *J. Biol. Chem.* **2011**, *286*, 41578–41588.
- [41] T. C. Lührs, C. Ritter, M. Adrian, D. Riek-Loher, B. Bohmann, H. Döbeli, D. Schubert, R. Riek, *Proc. Natl. Acad. Sci. USA* **2005**, *102*, 17342–17347.
- [42] D. S. Wishart, C. G. Bigam, A. Holm, R. S. Hodges, B. D. Sykes, *J. Biomol. NMR* **1995**, *5*, 67–81.
- [43] K. R. Harris, L. A. Woolf, *J. Chem. Eng. Data* **2004**, *49*, 1064–1069.
- [44] S. L. Stvolinsky, E. R. Bulygina, T. N. Fedorova, K. Meguro, T. Sato, O. V. Tyulina, H. Abe, A. Boldyrev, *Cell. Mol. Neurobiol.* **2010**, *30*, 395–404.
- [45] V. Lanza, F. Bellia, R. D'Agata, G. Grasso, E. Rizzarelli, G. Vecchio, *J. Inorg. Biochem.* **2011**, *105*, 181–188.

- [46] G. I. Grasso, G. Arena, F. Bellia, G. Maccarrone, M. Parrinello, A. Pietropaolo, G. Vecchio, E. Rizzarelli, *Chem. Eur. J.* **2011**, *17*, 9448–9455.
- [47] C. Corona, V. Frazzini, E. Silvestri, R. Lattanzio, R. La Sorda, M. Piantelli, L. M. T. Canzoniero, D. Ciavardelli, E. Rizzarelli, S. L. Sensi, *PLoS One* **2011**, *6*, e17971.
- [48] I. W. Hamley, *Chem. Rev.* **2012**, *112*, 5147–5192.
- [49] C. Rivière, T. Richard, L. Quentin, S. Krisa, J. M. Mérillon, J. P. Monti, *Bioorg. Med. Chem.* **2007**, *15*, 1160–1167.
- [50] V. S. Mithu, B. Sarkar, D. Bhowmik, M. Chandrakesan, S. Maiti, P. K. Madhu, *Biophys. J.* **2011**, *101*, 2825–2832.
- [51] B. O’Nuallain, A. K. Thakur, A. D. Williams, A. M. Bhattacharyya, S. Chen, G. Thiagarajan, R. Wetzel, *Methods Enzymol.* **2006**, *413*, 34–74.
- [52] M. G. Zagorski, J. Yang, H. Shao, K. Ma, H. Zeng, A. Hong, *Methods Enzymol.* **1999**, *309*, 189–204.
- [53] V. J. Garcia, L. Martinez, J. M. Briceño-Valero, C. H. Schilling, *Probe Microsc.* **1997**, *1*, 107–116.
- [54] B. Pignataro, L. Sardone, G. Marletta, *Nanotechnology* **2003**, *14*, 245–249.
- [55] B. Pignataro, *J. Mater. Chem.* **2009**, *19*, 3338–3350.
- [56] J. Vesenka, M. Guthold, C. L. Tang, D. Keller, E. Delaine, C. Bustamante, *Ultramicroscopy* **1992**, *42–44*, 1243–1249.
- [57] B. R. Brooks, R. E. Bruccolieri, B. D. Olafson, D. J. States, S. Swaminathan, M. Karplus, *J. Comput. Chem.* **1983**, *4*, 187–217.
- [58] B. R. Brooks, C. L. Brooks III, A. D. Mackerell Jr, L. Nilsson, R. J. Petrella, B. Roux, Y. Won, G. Archontis, C. Bartels, S. Boresch, A. Caflisch, L. Caves, Q. Cui, A. R. Dinner, M. Feig, S. Fischer, J. Gao, M. Hodoscek, W. Im, K. Kuczera et al., *J. Comput. Chem.* **2009**, *30*, 1545–1614.
- [59] U. Haberthür, A. Caflisch, *J. Comput. Chem.* **2008**, *29*, 701–715.
- [60] M. Seeber, A. Felline, F. Raimondi, S. Muff, R. Friedman, F. Rao, A. Caflisch, F. Fanelli, *J. Comput. Chem.* **2011**, *32*, 1183–1194.
- [61] M. Seeber, M. Cecchini, F. Rao, G. Settanni, A. Caflisch, *Bioinformatics* **2007**, *23*, 2625–2627.
- [62] W. Kabsch, C. Sander, *Biopolymers* **1983**, *22*, 2577–2637.
- [63] Y. Fezoui, D. M. Hartley, J. D. Harper, R. Khurana, D. M. Walsh, M. M. Condron, D. J. Selkoe, P. T. Lansbury, A. L. Fink, D. B. Teplow, *Amyloid* **2000**, *7*, 166–178.
- [64] L. Braunschweiler, R. R. Ernst, *J. Magn. Reson.* **1983**, *53*, 521–528.
- [65] J. Jeener, B. H. Meier, P. Bachmann, R. R. Ernst, *J. Chem. Phys.* **1979**, *71*, 4546–4553.
- [66] A. Bax, D. G. J. Davis, *J. Magn. Reson.* **1985**, *65*, 355–360.
- [67] D. Marion, K. Wüthrich, *Biochem. Biophys. Res. Commun.* **1983**, *113*, 967–974.
- [68] M. Piotto, V. Saudek, V. J. Sklenár, *J. Biomol. NMR* **1992**, *2*, 661–665.
- [69] T. L. Hwang, A. J. Shaka, *J. Magn. Reson. A* **1995**, *112*, 275–279.
- [70] K. F. Morris, C. S. Johnson, Jr., *J. Am. Chem. Soc.* **1992**, *114*, 3139–3141.
- [71] A. Jerschow, N. Müller, *J. Magn. Reson.* **1997**, *125*, 372–375.

---

Received: November 13, 2012

Published online on February 25, 2013